J Solid State Electrochem (2012) 16:1203–1210
DOI 10.1007/s10008-011-1473-x

ORIGINAL PAPER

Electrochemical fabrication of multiplicate palladium hierarchical architectures and their electrocatalysis toward oxidation of formic acid

Jia Chai · Fenghua Li · Yu Bao · Shiwei Liu · Qixian Zhang · Li Niu

Received: 30 June 2010 / Revised: 9 June 2011 / Accepted: 11 June 2011 / Published online: 29 July 2011

Abstract Dendritic, cactoid, splintery flowers-like and spinous flowers-like micro/nano-Pd hierarchical architectures were successfully deposited on the conductive substrates without assistance of any templates. Distinct from other general electrodeposition at a constant potential or cyclic potential, we utilized pulse potentials as deposition and dissolution potential, which were controlled by a simple and convenient electrochemical method—differential pulse amperometry. It was found that the morphologies of these novel micro/nanoparticles could be regulated with different pulse potentials. The resulting nanostructures were characterized by scanning electron microscopy and X-ray diffractometry. The results show that series of Pd micro/nanoparticles were bounded on the different index facets. It means that the growth direction could be effectively controlled by regulating the pulse potentials. Moreover, the as-synthesized Pd micro/nanoparticles also exhibited strikingly difference in catalytic activity toward electrooxidation of formic acid.

Keywords Pd micro/nanostructures · Differential pulse amperometry · Electrochemical deposition · Electrocatalysis · Formic acid

J. Chai · F. Li · Y. Bao · S. Liu · Q. Zhang (✉) · L. Niu
Engineering Laboratory for Modern Analytical Techniques,
c/o State Key Laboratory of Electroanalytical Chemistry,
Changchun Institute of Applied Chemistry,
Chinese Academy of Sciences,
Graduate University of the Chinese Academy of Sciences,
Changchun 130022 Jilin, Peoples Republic of China
e-mail: qxzhang@ciac.jl.cn

Introduction

Within the past decades, extensive researches have been carried out on Pd nanostructures with different morphologies and shapes due to their remarkable physical and chemical prosperities, which exhibit a broad application in the fields of hydrogen storage [1], gas sensors [2], biosensors [3], catalysis [4], etc. Among these various practical applications, catalysis such as electrochemical oxidation of methanol [5] and formic acid (FA) [6], precatalysis for Heck and Suzuki coupling reactions [7, 8] are most attractive for researchers. Pt is also a commonly used alternative catalyst in fuel cell reactions, especially in oxidation of FA. But recent progresses revealed that Pd nanoparticles can catalyze the oxidation of FA at the anode of direct formic acid fuel cells with greater resistance to CO than Pt catalysts [6], and Pd is much cheaper in the practical applications. Therefore, how to obtain the useful Pd nanoparticles and control the direction of growth are key problems for the scientists. It is considered that the morphology of nanoparticles determined the catalytic activity of products. Many kinds of Pd materials, including nanoparticles, nanorods [9], nanocubes [10], nanowires [11], nanoflowers [3], nanothorns [12], tetrahexahedral nanocrystals [13], and dendritic nanowires [14] were synthesized by various chemical and physical methods; however, only a few studies were relative to electrochemical approaches. Actually, electrochemical deposition is a convenient, environmental friendly, and time-saving method. However, it is complicated for colloidal chemistry strategy to assemble materials directly on the substrate, which is of significance for some applications, such as electrocatalysis, surface-enhanced Raman scattering, superhydrophobicity, etc. Several electrochemical approaches are applied to

synthesize multiplicate micro/nanostructures on the template [15] or with organic additives [16] and surfactants [17, 18]. Nevertheless, these methods could introduce impurities so that operation process became more tedious. Recently, some researchers devoted to studies of templateless and surfactantless electrochemical deposition on bare conductive substrates and obtained flower-like Au nanostructures [19] with square wave potential method. Moreover, it is reported [20] that nanostructures palladium deposits with region defectiveness fabricated by membrane separators. This method not only avoids introducing impurities but also improves the concern of layered metals. Even so, as far as we know, there is no report on differential pulse amperometry (DPA) to obtain various intact morphologies of Pd micro/nanoparticles directly on the substrates without assistance of any templates.

Herein, we reported a facile electrochemical deposition method to synthesize various Pd hierarchical architectures at different lower pulse potential (E_L) and upper pulse potential (E_U). As-synthesized products had a relatively higher stability. Even more interestingly, we found that the growth directions of these morphologies were changed by adjusting of E_L and E_U. Therefore, the required morphologies were synthesized easily and controllably. The prepared Pd nanostructures also exhibited different electrocatalytical activities toward the oxidation of FA and different degrees of CO poisoning.

Experimental

Materials

Sodium tetrachloropalladate (II) was purchased from Sigma-Aldrich Co., Ltd. Sulfuric acid and FA were purchased from Beijing Chemicals (Beijing, China). All reagents were used as received without further purification. The water used was purified through a Millipore system. Indium tin oxide (ITO) slides were cleaned in acetone, ethanol/H_2O 1:1 with some NaOH solution for 15 min each in an ultrasonic bath followed by washing in deionized water and drying in N_2 stream.

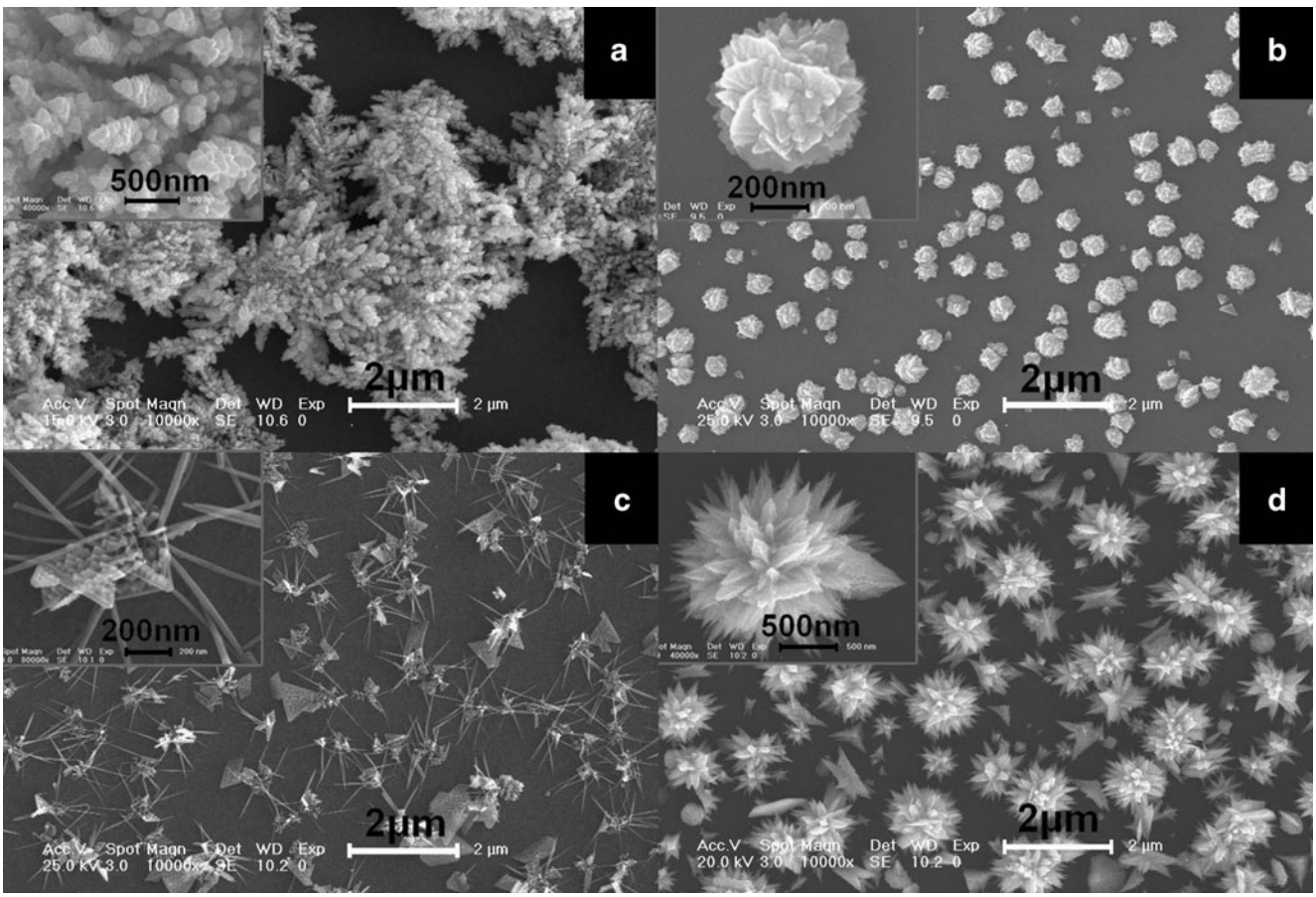

Fig. 1 SEM images of Pd nanostructures: **a** dendritic nanostructures prepared at E_L=−0.2 V, E_U=0.8 V; **b** splintery flowers-like nanostructures prepared at E_L=0 V, E_U=0.8 V; **c** cactoid nanostructures prepared at E_L=0.2 V, E_U=0.8 V; **d** spinous flowers-like nanostructures prepared at E_L=−0.2 V, E_U=1.2 V**.** Scan time is 12,000 cycles, respectively

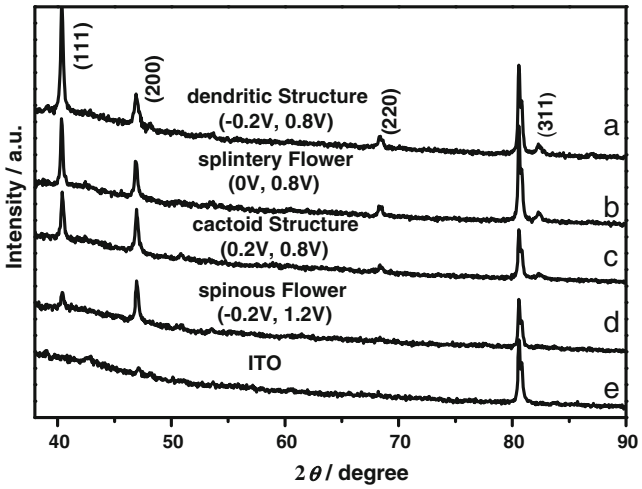

Fig. 2 Typical XRD patterns of Pd nanostructures obtained at **a** E_L=−0.2 V, E_U=0.8 V; **b** E_L=0 V, E_U=0.8 V; **c** E_L=0.2 V, E_U=0.8 V; **d** E_L=−0.2 V, E_U=1.2 V; and **e** ITO slides

Instruments

Scanning electron microscope (SEM) images were taken on XL30E SEM, and the accelerating voltage was 15 kV. X-ray diffraction (XRD) analysis was carried out on a D/Max 2500 V/PC X-ray diffractometer using Cu Kα (40 kV, 30 mA) radiation. Electrochemical experiments were performed with a CHI 660 electrochemical workstation (CHI Instruments, USA). The content of Pd atoms was obtained on an ICP spectrometer (ICAP 6000 Series, Thermo Scientific).

Preparation of Pd nanostructures and electrocatalysis

All various morphologies of Pd were electrochemically synthesized in a conventional three-electrode electrochemical cell using ITO slides as the working electrode at room temperature. The auxiliary electrode and counter electrode were made of an Ag|AgCl (in saturated KCl) electrode and a twisted platinum wire, respectively. All potentials in this work are referred to the Ag|AgCl reference electrode. In a general procedure, 0.5 M H_2SO_4 and 2 mM sodium tetrachloropalladate(II) (Na_2PdCl_4) solution were deaerated by N_2 bubbling for 20 min before electrodeposition. Pd nanoparticles were electrodeposited at DPA mode by the various pulse potential chosen between −0.2 and 1.2 V as E_L and E_U at 10 Hz for 12,000 cycles. After washing with deionized water and drying in a steam of N_2, the electrode was used for SEM and XRD characterizations and also directly for examination of catalytic oxidation of FA. The electrooxidation of FA was carried out in 0.5 M FA/0.5 M H_2SO_4 solution for 10 cycles at 50 mV s^{-1}. The electrolyte solution was also deaerated by N_2 bubbling for 20 min before the experiment.

Results and discussion

Figure 1a shows the SEM images of Pd nanostructures which were obtained with E_L=−0.2 V and E_U=0.8 V. The morphology of sample A (S_A) looks like branches assembled by ca. 50 nm Pd nanoparticles and width of each branch is ca. 1 μm. The hierarchical architectures are not uniform in dimension along both longitudinal and latitudinal axis. When E_L was improved to 0 V, the morphology was changed to splintery flowers-like (as shown in Fig. 1b). The as-synthesized particles were mono-disperse onto the ITO substrate, and the dimension of flowers was ca. 400 nm in diameter. Impressively the each nanostructure was assembled by leaf-like flakes with corrugate surface. As the E_L continuously increased to 0.2 V, we interestingly found that the further change happened (Fig. 1c). It is considered that the image of the sample C (S_C) is similar to cactuses, the small thorns out of the samples are not uniform due to their successive growth with time, and they are average 35 nm in diameters, approximately 0.7–1.5 μm in longitudinal. Comparing to the experimental conditions

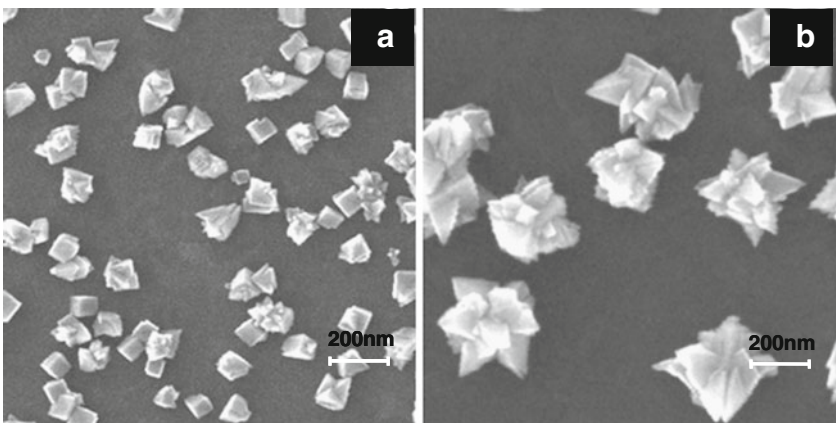

Fig. 3 SEM images of Pd nanostructures: **a** E_L=0 V, E_U=0.8 V. Scan time is 3,000 cycles; **b** E_L=0 V, E_U=0.8 V. Scan time is 6,000 cycles. Scan rate is 50 mV s^{-1}

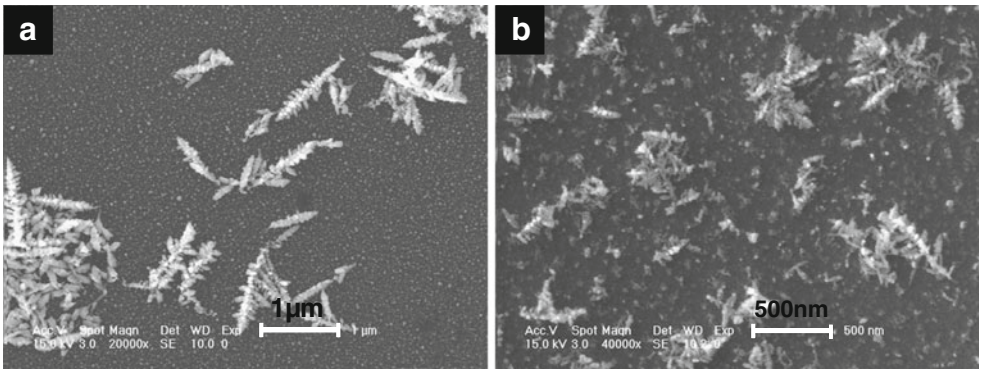

Fig. 4 SEM images of the Pd nanoparticles electrodeposited on glass carbon (**a**) and gold electrode (**b**) at E_L=−0.2 V, E_U=0.8 V

of the dendritic S_A, we applied the value of E_U to 1.2 V; sisal-like nanostructures (S_D) with ca. 1 μm diameter were obtained. However, there were some small size fragments on the substrates. Therefore, the shape and morphologies of the Pd nanostructures could be adjusted by choosing the suitable pulse potential. As known, E_L is the depositing voltage and E_U is stripping voltage. It is a circular and reciprocating process with continuous depositing and stripping during the whole electrochemical synthesis. Increasing the value of E_L, the trends in the deposition of palladium ions was weaken; while increasing the value of the E_U, the trends in stripping or dissolution was further enhanced. So the amounts of deposition on the ITO substrates and the growth direction are influenced significantly by the pulse potential. From those SEM images of S_A, S_B, and S_C, the distribution densities of these Pd hierarchical architectures gradually increased (S_A>S_B>S_C). As shown in the XRD results (Fig. 2) in the range of 35°< 2θ<85°, the peaks, located at 40.34°, 46.89°, 68.39°, and 82.30°, are assigned to (111), (200), (220), and (311) faces, which are the typical Pd structures. The lattice parameter of α=0.387 nm by calculating which is in accordance with the

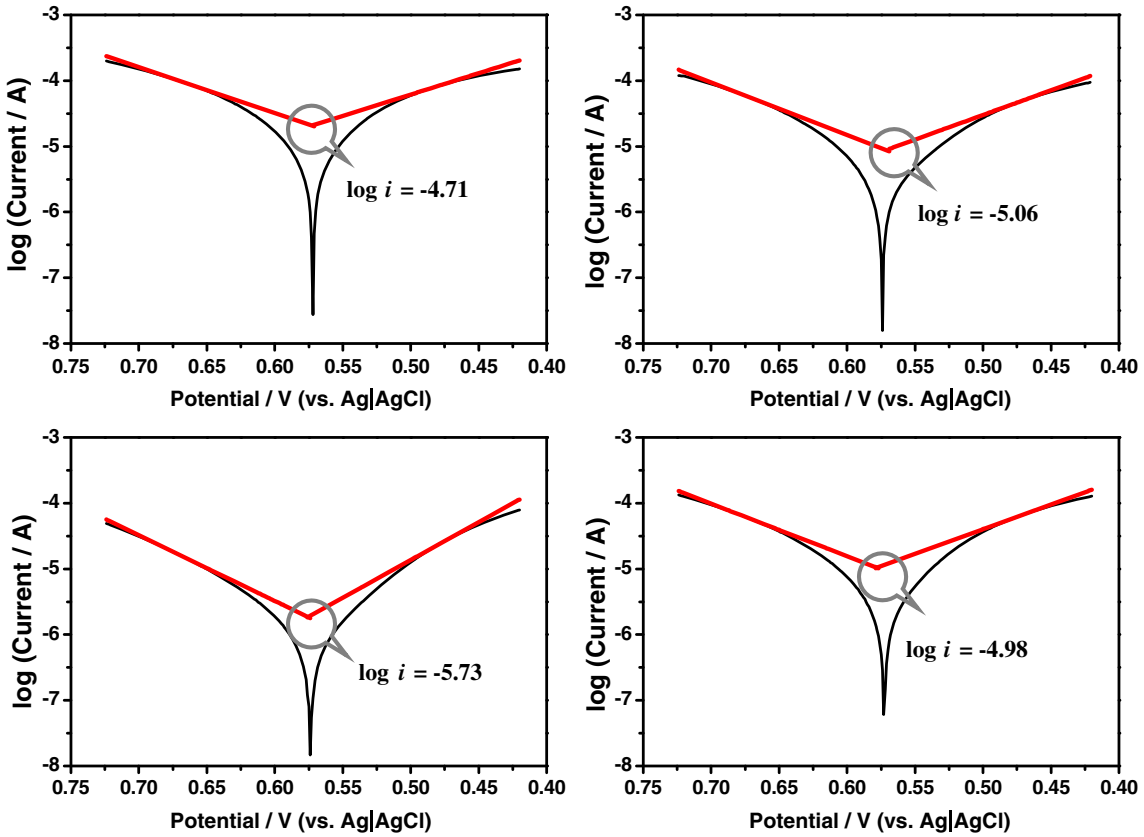

Fig. 5 Tafel polarization curve of Pd in 0.5 M H_2SO_4 containing 2 mM Na_2PdCl_4. The working electrode was obtained by deposition in the same solution at **a** E_L=−0.2 V, E_U=0.8 V; **b** E_L=0 V, E_U=0.8 V; **c** E_L=0.2 V, E_U=0.8 V; and **d** E_L=−0.2 V, E_U=1.2 V for 3,000 cycles, respectively. Scan rate is 10 mV s^{-1}

Joint Committee Powder Diffraction Standard of bulk Pd (no. 87-0645). It could be found that when the depositing voltage E_L was increased from −0.2 to 0 and to 0.2 V, the ratio of peak height of (111) to (200) decreased from 3.34, 1.84 to 1.09. In other words, the growth directions were gradually changed from (111) facet to (200) facet with the increase of the value of E_L. From the SEM and XRD comparison of S_A and S_D, the (200) facet became a dominant direction of crystal growth due to the increase of stripping voltage. Consequently, a simple schematic diagram (Fig. 1e) of growth mechanism base on the crystal orientation was illustrated. The degree of the deposition was increased, and (111) facet is dominant in growth of Pd nanostructures; while the abilities of the stripping were increased, (200) facet is a predominant direction during the processes of growth. Additionally, as-prepared Pd hierarchical architectures were stable in air at room temperature at least for 6 weeks.

In order to further explore the growth process of Pd nanoparticles, the nanostructures against different numbers of cycles was also studied (Fig. 3). We take the samples which is deposited with E_L=0 V and E_U=0.8 V as example. At 3,000 cycles, a series of ca. 100 nm irregular Pd nanoparticles with small edges and corners were deposited on the ITO slide (Fig. 3a). With the number of cycles increasing up to 6,000, the dimension of the nanoparticles was increased to ca. 250 nm, and the flower-like Pd nanoparticles were gradually emerged (Fig. 3b). When the cycle number arises to 12,000, spinous flowers-like Pd nanostructures are obtained. If improving the cycles continuingly, it was found that the dimension and the density of the nanostructures were increased, but the morphology of the sample remained stable. Additionally, we have measure the mass of palladium deposited through the different cycles. First, the palladium was deposited on the ITO slide with fixed 5 mm diameter at E_L=0 V, E_U= 0.8 V in 3,000, 6,000, and 12,000 cycles, respectively. After washing with deionized water and drying in a steam of N_2, the palladium was dissolved from ITO slide with aqua regia. The solutions with palladium ions were measured by ICP.The concentrations of the samples with 3,000, 6,000, and 12,000 cycles successively were 1,399, 2,267, and 4,827 ppb. Comparing the data, it was considered that the mass of palladium depositing in early 6,000 cycles were slightly lower than that depositing in later 6,000 cycles.

Investigating the effect of the substrates on the morphology, we choose glass carbon (GC) and gold electrode (GE) for comparison in the same conditions, including methods, concentration and component of the solution, the potential of deposition and scanning time, etc. Figure 4 shows SEM

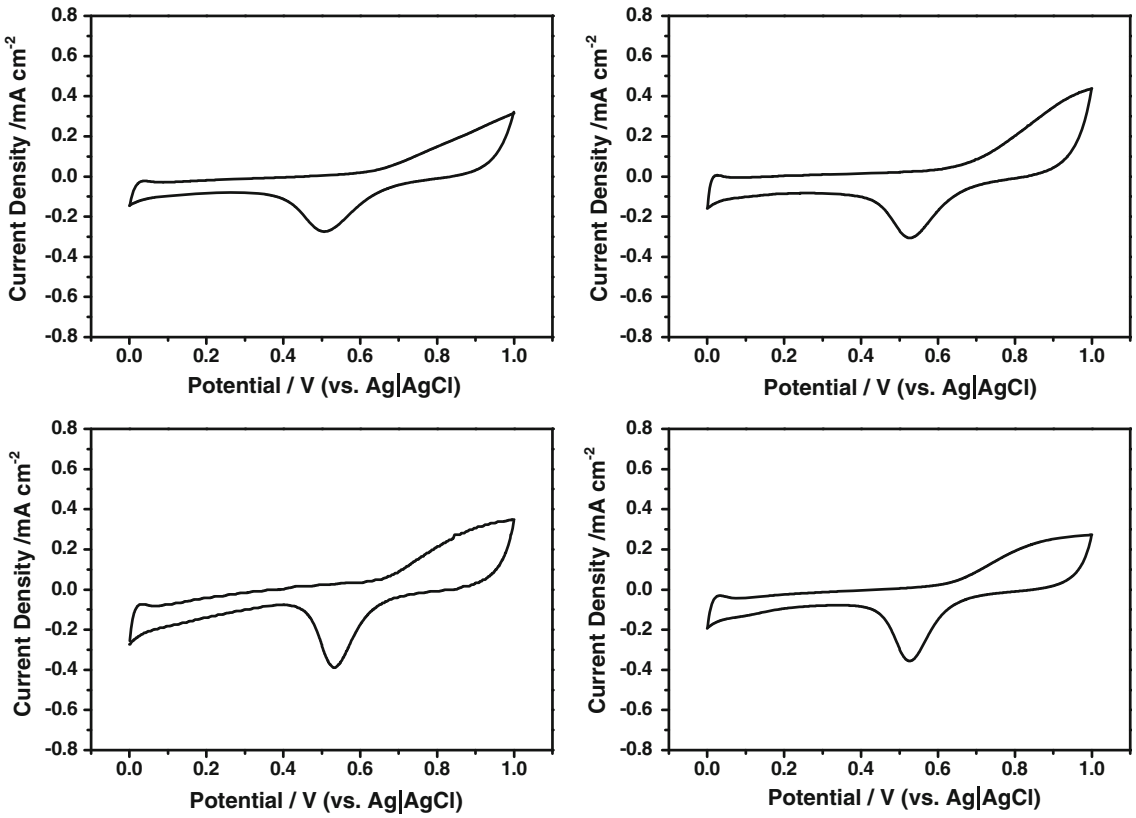

Fig. 6 Normalized CVs of the Pd with various morphologies obtained in 0.5 M H_2SO_4 at **a** E_L=−0.2 V, E_U=0.8 V; **b** E_L=0 V, E_U=0.8 V; **c** E_L= 0.2 V, E_U=0.8 V; and **d** E_L=−0.2 V, E_U=1.2 V. Scan rate is 50 mV s^{-1}

images of Pd nanostructures prepared at E_L=−0.2 V, E_U= 0.8 V on the GC (A) and GE (B), respectively. From Fig. 4, the dendritic Pd nanoparticles can be found on the GC and GE (gold slice), and the dimension of the branch is not uniform, ca. 0.7~1.0 and 0.3–0.5 μm along the longitudinal, respectively. The morphologies of these samples were similar with the S_A only with smaller volume and less quantity. It is noted that some irregularly Pd nanoparticles, ca. 20~35 nm in size, were scattered on the substrate. We considered that the surface roughness of both GC and GE influence the growth rates so that the crystals remain staying at the initial growth stages. Comparing with the SEM images of S_A, we believed the electrodeposition is a very sensitive technique [21]. However, in this system, the choice of substrate is a not decisive factor on the initial growth of nanoparticles during the process of electrodeposition. The pulse potential controlled the initial growth and morphologies of Pd nanoparticles. The (111) facet of dendritic Pd nanoparticles is still dominant growth direction.

The Tafel plots can be used to provide information about the kinetics of the electron transfer reaction. Discussing the kinetic of palladium deposition and dissolution, we used ITO slides as the working electrodes which were inserted in 2 mM Na_2PdCl_4 and 0.5 M H_2SO_4 mixing solution with electrodepositing at corresponding potentials for 3,000 cycles. The scan rate is 50 mV s^{-1}. Then, we got the corresponding Tafel plots (Fig. 5) in same solution with the scan rate of 50 mV s^{-1}. The plots were approximate symmetric. By calculating on Tafel slopes, transfer coefficient (α) are in sequence of 0.48, 0.48, 0.53, and 0.48, respectively. For simple consideration, the deposition/dissolution processes were approximately considered to be a simple single-step transfer of two electrons in our system. So, we could calculate the standard rate constant k_0 in different system by Eq. 1 of exchange current (i_0)

$$i_0 = nFAk_0 C_O^{*(1-\alpha)} C_R^{*\alpha} \quad (1)$$

where n is the number of electron; C_O and C_R represent the concentrations of oxidized and reduced states, respectively; and A is the electrode area which is a diameter of 6 mm in our system. By calculating, the k_0 is of the order of 10^{-10}–10^{-9} cm/s. It seems that the reaction of Pd deposition/dissolution is slower. So, we speculated that the growth of crystal and the formation of the morphologies mainly accord with crystal growth kinetics. During the electrochemical process up to E_U, the oxygen would be diffused or

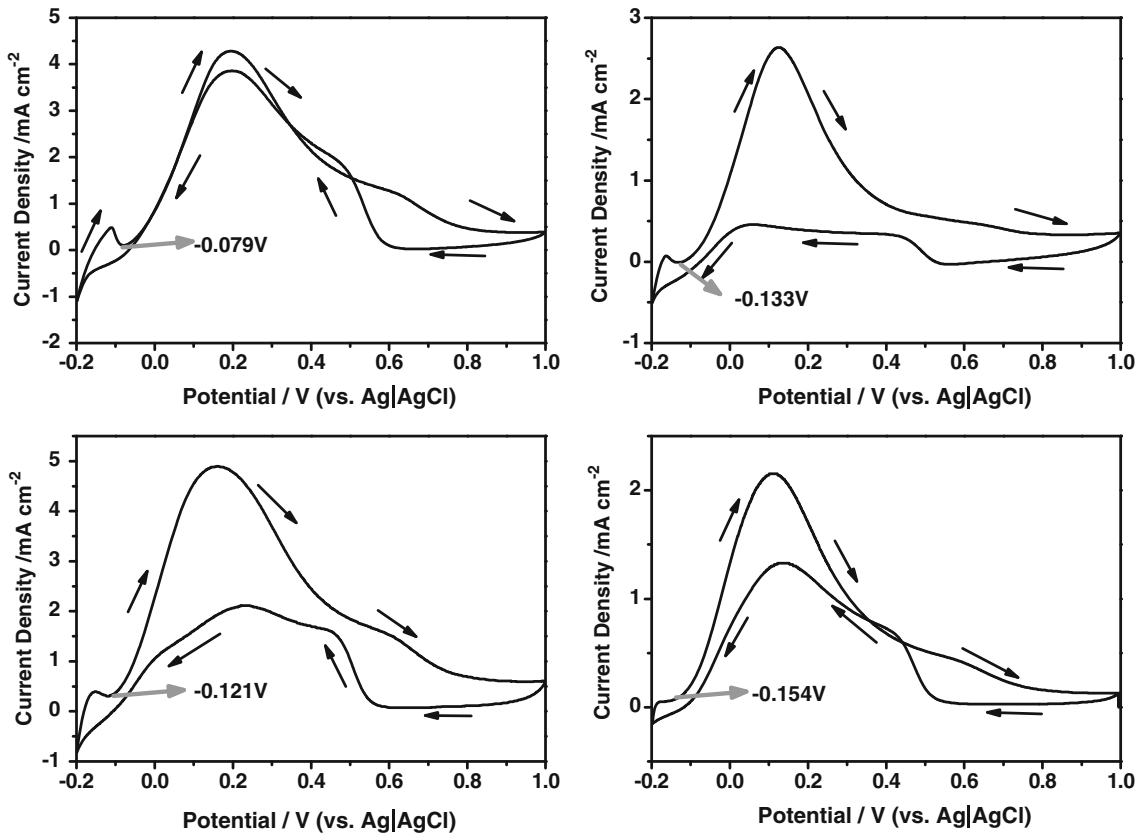

Fig. 7 Normalized CVs for electrooxidation of 0.5 M FA in 0.5 M H_2SO_4 on the Pd catalyst prepared at **a** E_L=−0.2 V, E_U=0.8 V; **b** E_L=0 V, E_U= 0.8 V; **c** E_L=0.2 V, E_U=0.8 V; and **d** E_L=−0.2 V, E_U=1.2 V. Scan rate is 50 mV s^{-1}. Start potential was pointed out in figures, respectively

invade into the crystal lattices with lower energy while the unstable Pd atom dissolved from the higher energy crystal facet into the solution. When at E_U, the oxygen atom would be desorbed from the lattices while Pd atoms returned to original positions or other lattices with lower energy [9, 22]. Therefore, the crystal depositing at the different potentials would grow according to a certain direction which leads to achieve the more stable state.

Cyclic voltammetry (CVs) of the Pd with different morphologies in background solution (0.5 M H_2SO_4) are showed in Fig. 6. Scan rate is 50 mV s^{-1}. Profile differences show in the CVs of these samples. The negative-going curve of S_A to S_D presents a reduction peak at 0.37, 0.42, 0.46, and 0.47 V, respectively. Electrocatalytic activities of the Pd micro/nanostructures were examined by CVs in a FA/H_2SO_4 solution. To exactly evaluate the electrocatalysis, all current densities at the Pd catalysts were normalized by real surface area. Usually, we utilized the oxygen adsorption method to evaluate electrochemical active surface areas of metals showing well-developed regions for oxide monolayer formation and reduction [23], such as Au and Pd. So, we estimated from the charge needed to form surface oxide monolayer that the conversion factor is 424 μC cm^{-2} [5, 24]. The reduction charge of Pd surface oxide is integrated to be 403.0, 158.32, 50.08, and 114.1 μC from S_A to S_D. Divided by conversion factor, the corresponding active surface area is 0.95, 0.374, 0.118, and 0.27 cm^2, respectively.

Figure 7 shows the CVs of the FA oxidation on Pd catalysts with different morphologies. All of the four curves show obvious oxidation peaks and minor hump at around 0.6 V between the positive potential excursions, which are related to the direct oxidation of FA and the oxidation of Pd [12]. The start potential was signed out. During the subsequent negative excursion, broad oxidation peak appeared obviously which reflected the stripping of the absorbed intermediates and regeneration of the Pd surface [5, 25]. But there were obvious differences of those in peak currents and poisoning degree of the electrode. Based on the current densities, S_C exhibited the maximum activity for FA oxidation in the CVs clearly. As mentioned above, the oxidation of FA at Pt particles and other noble metals is strongly hindered by CO poisoning because of formation of intermediate on the first step of the oxidation. Evident oxidation of FA occurs in the negative excursion after the intermediate is oxidized and removed at the lower potential [26]. It is observed from the CVs clearly that dendritic-like S_A has the highest reverse current in these four samples, which demonstrate that S_A has the lowest extent of the surface blocking with adsorbed CO and the highest ability of anti-poisoning [27, 28]. From the analysis, the factors including the current densities and the degree of poisoning in the electrode, which affect the electrocatalytic activity of various Pd particles, were regulated by the morphologies and structures of the samples. Furthermore, the surface electronic structures of metal Pd, which lead to form various morphologies, determine the activity of the catalyst [29].

Conclusions

In sum, a convenient electrochemical method—DPA—has been developed to synthesize structurally diverse Pd hierarchical architectures with different pulse potential. The integrity and diversity of micro/nanostructures are worth mentioning, and the formation along different facet is attributed to the oxidation activity of the Pd surface which is changed with the E_L and E_U. Different morphologies of the Pd have distinction of the catalytic properties to the oxidation of FA. The results also indicated that the simple method not only tunes the shapes and morphologies effectively but also synthesizes purposefully Pd micro/nanoparticles in various research areas. Thus, the developed method has great potential in the synthesis of hierarchical architectures and further in directed synthesis. Furthermore, the method can provide a highly rough platform easily to form composite nanostructures for other applications, such as surface-enhanced Raman spectroscopy.

Acknowledgments The authors are most grateful to the NSFC, China (No. 20827004), the Department of Science and Technology of Jilin Province (No. 20080518), and Chinese Academy of Sciences (YZ200906, YZ2010018, and KGCX2-YW-231) for their financial support.

References

1. Langhammer C, Zorić I, Kasemo B, Clemens BM (2007) Nano Lett 7(10):3122–3127
2. Favier F, Walter EC, Zach MP, Benter T, Penner RM (2001) Science 293(5538):2227–2231
3. Zhou P, Dai Z, Fang M, Huang X, Bao J, Gong J (2007) J Phys Chem C 111(34):12609–12616
4. Stahl SS (2005) Science 309(5742):1824–1826
5. Pan W, Zhang X, Ma H, Zhang J (2008) J Phys Chem C 112 (7):2456–2461
6. Mazumder V, Sun S (2009) J Am Chem Soc 131(13):4588–4589
7. Phan NTS, Van Der Sluys M, Jones CW (2006) Adv Synth Catal 348(6):597
8. Primo A, Liebel M, Quignard F (2009) Chem Mater 21(4):621–627
9. Tian N, Zhou ZY, Sun SG (2009) Chem Commun 12:1502–1504
10. Lim B, Jiang M, Tao J, Camargo PHC, Zhu YM, Xia YN (2009) Adv Funct Mater 19(2):189–200
11. Xu CW, Wang H, Shen PK, Jiang SP (2007) Adv Mater 19 (23):4256–4259
12. Meng H, Sun S, Masse JP, Dodelet JP (2008) Chem Mater 20 (22):6998–7002

13. Tian N, Zhou ZY, Wang LY, Yu NF, Sun SG (2010) J Am Chem Soc 132(22):7580–7581
14. Song YJ, Kim JY, Park KW (2008) Cryst Growth Des 9(1):505–507
15. Cheng FL, Wang H, Sun ZH, Ning MX, Cai ZQ, Zhang M (2008) Electrochem Commun 10(5):798–801
16. Ananikov VP, Orlov NV, Beletskaya IP, Khrustalev VN, Antipin MY, Timofeeva TV (2007) J Am Chem Soc 129(23):7252–7253
17. Chauhan BPS, Rathore JS, Bandoo T (2004) J Am Chem Soc 126 (27):8493–8500
18. Jia FL, Wong KW, Du RX (2009) Electrochem Commun 11 (3):519–521
19. Wang L, Guo S, Hu X, Dong S (2008) Electrochem Commun 10 (1):95–99
20. Frydrychewicz A, Biegunski AT, Jackowska K, Tsirlina GA (2008) J Solid State Electrochem 12(9):1085–1091
21. Huang XJ, Yarimaga O, Kim JH, Choi YK (2009) J Mater Chem 19(4):478–483
22. Tian N, Zhou ZY, Sun SG (2008) J Phys Chem C 112(50):19801–19817
23. Wang XG, Wang WM, Qi Z, Zhao CC, Ji H, Zhang ZH (2009) Electrochem Commun 11(10):1896–1899
24. Trasatti S, Petrii OA (1991) Pure Appl Chem 63(5):711–734
25. Zhang J, Qiu C, Ma H, Liu X (2008) J Phys Chem C 112 (36):13970–13975
26. Lee H, Habas SE, Somorjai GA, Yang P (2008) J Am Chem Soc 130(16):5406–5407
27. Zhou Y, Liu J, Ye J, Zou Z, Ye J, Gu J, Yu T, Yang A (2010) Electrochim Acta 55(17):5024–5027
28. Jayashree RS, Spendelow JS, Yeom J, Rastogi C, Shannon MA, Kenis PJA (2005) Electrochim Acta 50(24):4674–4682
29. Dekker M (1976) Electroanalytical chemistry, vol 9. Basel, New York